5th Australasian Congress on Applied Mechanics, ACAM 2007
10-12 December 2007, Brisbane, Australia

An Improved Flexibility Formulation for Nonlinear Analysis of Reinforced Concrete Frames

H. R. Vali pour[1] and S. J. Foster[2]

[1]*Research student, School of Civil and Environmental Engineering, University of New South Wales, NSW, Australia*
[2]*A/Prof., School of Civil and Environmental Engineering, University of New South Wales, NSW, Australia*

Abstract: In this paper the finite element flexibility-based formulation for a reinforced concrete frame element is discussed. The formulation takes account of material non-linearity on the basis of the one-dimensional stress-strain relationships akin to the traditional fibre element. However, the fibres in this method are replaced by transverse integration points to improve the efficiency of the method. The compatibility of strain in each section is satisfied by adopting the Navier-Bernoulli hypothesis and effect of shear tractions on the nonlinear response of the material is neglected. Two different iterative solution strategies based on secant and tangent stiffness, consistent with the flexibility formulation are employed for solving the governing equation. The accuracy of assumptions and performance of the solution schemes are studied by a numerical example.

Keywords: finite element, flexibility matrix, monotonic loading, Navier-Bernoulli hypothesis.

1 Introduction

Among existing finite element models (i.e. global, discrete and microscopic models) discrete models are a good compromise between accuracy and simplicity which is the focus of this study.

Nonlinearity of a discrete frame element can be formulated in the framework of a lumped or distributed model, where lumped models consist of a frame element with two nonlinear rotational/translational springs (nodes) at each end [1-3] . Despite their usefulness, nonlinear lumped models typically suffer three main problems, zero length of plastic hinges, priori assumptions for determining model parameters and ample diversity of these parameters required for calibration of model. While, introducing a plastic hinge length obtained from an empirical relationship may alleviate the first problem, this technique for members experiencing extensive damage or plasticity, such as a beam-column with high axial force, is not adequate [4]. Thus, the idea of distributed nonlinearity was proposed to overcome the inherent deficiencies in the lumped approach.

The first elements with distributed nonlinearity took advantage of the classical stiffness method based on a predefined Hermitian displacement shape function [5, 6]. The assumption of cubic Hermitian displacement interpolation results in a linear curvature distribution, hence, the abrupt change of curvature over the inelastic hinge zone can not be captured accurately unless mesh refinement is carried out over the inelastic zone. Obviously, mesh refinement and application of higher order displacement shape functions will increase the accuracy but also increases the analysis time.

Generally, the stiffness and flexibility method have the same degree of approximations. However, in frames, adopting some kinematic assumptions with the flexibility formulation uncouples the equilibrium equations from compatibility and they can be satisfied exactly. In such a case the efficiency of the formulation is improved without increasing the number of degrees of freedom per element. The first application of flexibility dependent shape functions that are updated continuously dates back to the early 1980s [7]. Since then the flexibility formulation has been used for static/cyclic or dynamic analysis of frames, including different type of material and geometrical nonlinearities [8-11]. In parallel with flexibility-based elements, appropriate solution schemes consistent with flexibility have been developed. These solution strategies mostly comprise two loops, one for iteration at element level and a second for iteration at the structure level [11, 12].

In this paper the efficiency of the flexibility method is improved by employing a numerical integration at section level rather than fibre discretization. Two different solution strategies based on tangent and secant stiffness are employed for solving the governing equation and the influence of numerical integration order and solution scheme on the formulation accuracy and efficiency is examined.

2 Flexibility formulation of the beam-column element

In this study a cantilever clamped end configuration is used for deriving the element stiffness (flexibility) matrixes (Figure 1a).

2.1 Equilibrium equations at element and section level

Figure 1b depicts a 2-node frame element AB with six degrees of freedom at each node (three translations and three rotations) subjected to the distributed loads $w_y(x)$ and $w_z(x)$. If the torsional DOFs are neglected in the element formulation, then equilibrium for configuration Ax (Figure 1b) gives

$$\mathbf{D}(x) = \mathbf{b}(x)\,\mathbf{Q}_A + \mathbf{D}^*(x) \tag{1}$$

$$\mathbf{D}^*(x) = \begin{bmatrix} 0 & -M_z^*(x) & -M_y^*(x) \end{bmatrix}^T \tag{2}$$

$$\mathbf{b}(x) = \begin{bmatrix} -1 & 0 & 0 & 0 & 0 \\ 0 & x & 0 & -1 & 0 \\ 0 & 0 & -x & 0 & -1 \end{bmatrix} \tag{3}$$

where, $\mathbf{Q}_A = \begin{bmatrix} Q_1 & Q_2 & Q_3 & Q_4 & Q_5 \end{bmatrix}^T$ and $\mathbf{D}(x) = \begin{bmatrix} N(x) & M_z(x) & M_y(x) \end{bmatrix}^T$ denote the vector of element generalized forces at end A and section generalized force, $\mathbf{b}(x)$ is the force interpolation matrix and $\mathbf{D}^*(x)$ is sectional internal force vector solely due to the distributed loads $w_y(x)$ and $w_z(x)$.

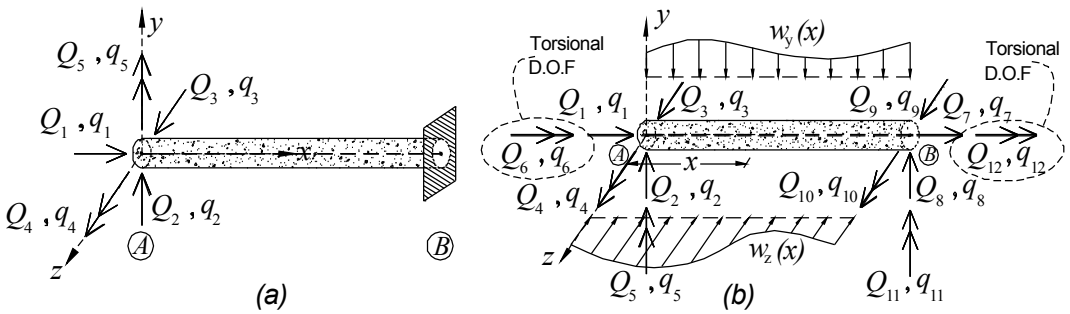

Figure 1 (a) Cantilever configuration used for deriving the flexibility equations (b) 3D frame element and corresponding DOF.

Removing the term $\mathbf{D}^*(x)$ from (1) does not violate the generality of the formulation and, hence

$$\mathbf{D}(x) = \mathbf{b}(x)\,\mathbf{Q}_A \tag{4}$$

If s represents the stress at a transverse integration point on the section, then equilibrium of internal stresses and section internal tractions gives

$$\int_\Omega \mathrm{s}\; dA - N(x) = 0 \tag{5}$$

$$\int_\Omega y\;\mathrm{s}\; dA + M_z(x) = 0 \tag{6}$$

$$\int_\Omega z\;\mathrm{s}\; dA + M_y(x) = 0 \tag{7}$$

In (5) to (7), the stress is replaced by stress increment, $\Delta\mathrm{s}$, the section internal forces are replaced by their increment $(\Delta N, \Delta M_y, \Delta M_z)$ and the incremental form of the section equilibrium is obtained.

2.2 Compatibility equations

Adopting the Navier-Bernoulli hypothesis, the compatibility requirement is obtained as

$$\mathsf{e}(x) = \mathsf{e}_r(x) - y\,\mathsf{k}_z(x) - z\,\mathsf{k}_y(x) \tag{8}$$

where, $\mathsf{e}(x)$ denotes the total axial strain of the fibre or integration point and the increment of this axial strain is, $\Delta\mathsf{e}(x) = \Delta\mathsf{e}_r(x) - y\,\Delta\mathsf{k}_z(x) - z\,\Delta\mathsf{k}_y(x)$.

2.3 Constitutive law and section stiffness matrix

The constitutive law of material can be expressed using the total stress-strain relationship (Figure 2a)

$$\mathsf{s} = E_e\,(\mathsf{e} - \mathsf{e}_p) \tag{9}$$

or in a linearized incremental form (Figure 2b)

$$\Delta\mathsf{s} = E_t\,.\,\Delta\mathsf{e} \tag{10}$$

where E_t and E_e are material tangent and secant modulus, respectively.

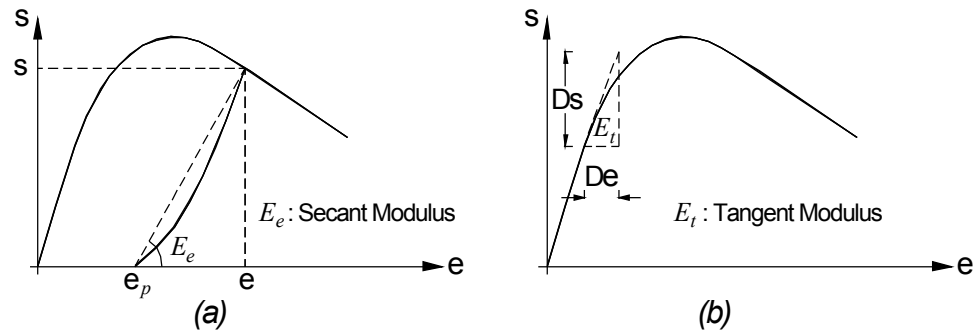

Figure 2 Constitutive law (a) linear Incremental (b) total Stress-strain relationship.

Substituting the compatibility equation and constitutive law in (5) to (7) yields [13]

$$\mathbf{D}(x) = {}^{e}\mathbf{k}_s(x)\,\mathbf{d}(x) + \mathbf{D}_p(x) = \left[{}^{e}\mathbf{f}_s(x)\right]^{-1}\mathbf{d}(x) + \mathbf{D}_p(x) \tag{11}$$

$$\Delta\mathbf{D}(x) = {}^{t}\mathbf{k}_s(x)\,\Delta\mathbf{d}(x) = \left[{}^{t}\mathbf{f}_s(x)\right]^{-1}\Delta\mathbf{d}(x) \tag{12}$$

$$\mathbf{D}_p(x) = \left[-\int_\Omega E_e\,.\mathsf{e}_p\,dA \quad \int_\Omega y\,E_e\,.\mathsf{e}_p\,dA \quad \int_\Omega z\,E_e\,.\mathsf{e}_p\,dA\right]^T \tag{13}$$

$${}^{s(t)}\mathbf{k}_s(x) = \left[{}^{s(t)}\mathbf{f}_s(x)\right]^{-1} = \begin{bmatrix} \int_\Omega E_{e(t)}\,dA & -\int_\Omega y\,E_{e(t)}\,dA & -\int_\Omega z\,E_{e(t)}\,dA \\ -\int_\Omega y\,E_{e(t)}\,dA & \int_\Omega y^2\,E_{e(t)}\,dA & \int_\Omega yz\,E_{e(t)}\,dA \\ -\int_\Omega z\,E_{e(t)}\,dA & \int_\Omega yz\,E_{e(t)}\,dA & \int_\Omega z^2\,E_{e(t)}\,dA \end{bmatrix} \tag{14}$$

where, ${}^{e(t)}\mathbf{k}_s(x)$ and ${}^{e(t)}\mathbf{f}_s(x)$ are section stiffness and flexibility matrixes ,respectively, and $\mathbf{D}_p(x)$ denotes the residual plastic force vector for the section. The left superscript e and t denote the secant and tangent counterpart of quantities (equations), correspondingly.

If the stiffness matrix of the element AB is denoted by ${}^{e(t)}\mathbf{K}_e$ and k_t represent the torsional stiffness of the element, adopting the torsions as independent of the other tractions gives [13]

$$ {}^{e(t)}\mathbf{K}_e = \begin{bmatrix} \left[{}^{e(t)}\mathbf{F}_{AA}\right]^{-1} & \mathbf{0} & {}^{e(t)}\mathbf{K}_{AB} & \mathbf{0} \\ \mathbf{0}^T & k_{\mathrm{t}} & \mathbf{0}^T & k_{\mathrm{t}} \\ {}^{e(t)}\mathbf{K}_{AB}^T & \mathbf{0} & {}^{e(t)}\mathbf{K}_{BB} & \mathbf{0} \\ \mathbf{0}^T & k_{\mathrm{t}} & \mathbf{0}^T & k_{\mathrm{t}} \end{bmatrix} \tag{15} $$

Using the principle of virtual work for the cantilever configuration AB clamped at end B and subjected to a virtual load vector $\mathbf{Q}_A\,(\Delta\mathbf{Q}_A)$ at end A (Figure 1a), together with (4), (11) and (12) gives [13]

$$ \mathbf{q}_p = \int_0^l \mathbf{b}^T(x)\ {}^{e}\mathbf{f}_s(x)\ \mathbf{D}_p(x)\ dx \tag{16} $$

$$ {}^{e(t)}\mathbf{F}_{AA} = \left[{}^{e(t)}\mathbf{K}_{AA}\right]^{-1} = \int_0^l \mathbf{b}^T(x)\ {}^{e(t)}\mathbf{f}_s(x)\ \mathbf{b}(x)\ dx \tag{17} $$

where $\mathbf{q}_p$ is nodal generalised plastic displacements vector at end A, and it is related to element internal nodal plastic force vector $\mathbf{Q}_p$, by

$$ \mathbf{Q}_p = \begin{bmatrix} \mathbf{Q}_{p\,(A)} \\ \mathbf{\Gamma}^T\ \mathbf{Q}_{p\,(A)} \end{bmatrix} \tag{18} $$

Repeating the same procedure for a cantilever clamped at end A and subjected to a virtual load vector $\mathbf{Q}_B\,(\Delta\mathbf{Q}_B)$ at end B gives the stiffness sub-matrices (i.e. ${}^{e(t)}\mathbf{K}_{AA}$, ${}^{e(t)}\mathbf{K}_{AB}$, ${}^{e(t)}\mathbf{K}_{BB}$) interrelationship which is condensed as follows

$$ {}^{e(t)}\mathbf{K}_e = \begin{bmatrix} \left[{}^{e(t)}\mathbf{F}_{AA}\right]^{-1} & \mathbf{0} & \left[{}^{e(t)}\mathbf{F}_{AA}\right]^{-1}\mathbf{\Gamma} & \mathbf{0} \\ \mathbf{0}^T & k_{\mathrm{t}} & \mathbf{0}^T & k_{\mathrm{t}} \\ \mathbf{\Gamma}^T\left[{}^{e(t)}\mathbf{F}_{AA}\right]^{-1} & \mathbf{0} & \mathbf{\Gamma}^T\left[{}^{e(t)}\mathbf{F}_{AA}\right]^{-1}\mathbf{\Gamma} & \mathbf{0} \\ \mathbf{0}^T & k_{\mathrm{t}} & \mathbf{0}^T & k_{\mathrm{t}} \end{bmatrix} \tag{19} $$

$$ \mathbf{\Gamma} = \begin{bmatrix} -1 & 0 & 0 & 0 & 0 \\ 0 & -1 & 0 & L & 0 \\ 0 & 0 & -1 & 0 & -L \\ 0 & 0 & 0 & -1 & 0 \\ 0 & 0 & 0 & 0 & -1 \end{bmatrix} \tag{20} $$

3 Solution strategies

Two different solution strategies correspond with tangent and secant stiffness approach is used in this study. The first one is based on the modified nested iterative algorithm which employs the tangent stiffness [12]. The second scheme is a nested iterative algorithm that takes advantage of direct iteration in accompany with secant stiffness [13]. A convergence criterion based on the infinite norm of displacements is used at the structure level with a tolerance of 0.05%.

4 Numerical example

Figure 3 shows the geometry and loading of a simply supported beam tested by Burns and Siess [14]. The measured material properties for the specimen were $f_y = 310$ MPa (yield stress of steel bars), $E_s = 2.03\times10^5$ MPa (steel modulus of elasticity), $f_{cp} = 33$ MPa (concrete compressive strength),

$E_c = 2.62\times10^4$ MPa (concrete modulus of elasticity), and the tensile strength is taken as $f_t = 0.4\sqrt{f_{cp}} = 2.3$ MPa.

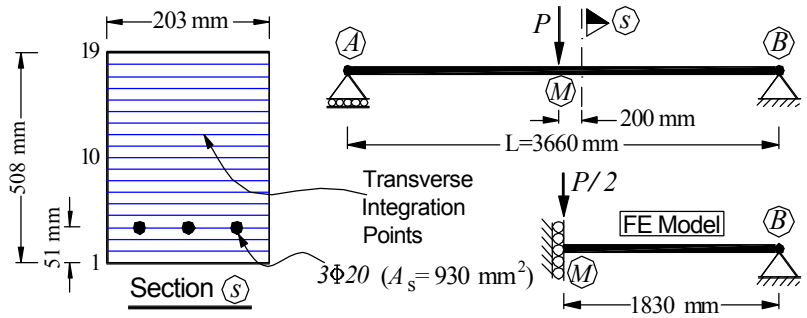

Figure 2 Simple span beam and section geometry along with idealized FE model.

One half of the beam is modelled by a single flexibility-based element (Figure 3). Different integration schemes with different numbers of longitudinal integration points are used to analyse the beam while a composite Simpson's method with 19 transverse integration points taken through the section height is used (Figure 4). The Results are compared with the 2D SBETA finite element membrane model of ATENA using a rotating crack with variable shear retention factor and element size of 25 mm.

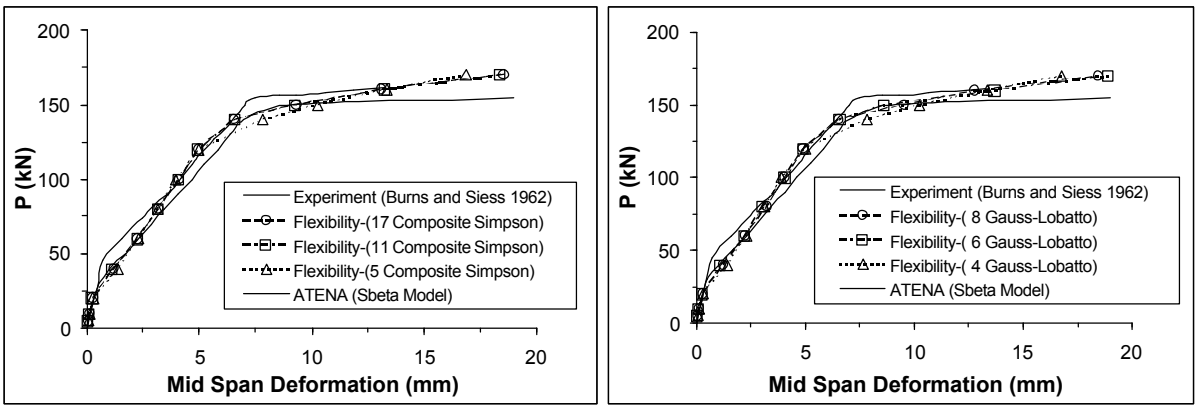

(a) *(b)*

Figure 4 Load versus mid-span deflection obtained from (a) composite Simpson (b) Gauss-Lobatto scheme within different number of longitudinal integration points.

In Figure 4, the results of tangent and secant stiffness approaches have not been depicted separately as they are the same up to 4 digits. Tables 1 and Table 2 show the number of iterations required for convergence at different load steps together with the total time of analysis on a notebook computer with a 1.6 MHz Intel Pentium M processor, within various integration points and solution schemes. The load steps are not equal and time of analysis denotes the total processing time spent for the entire load-deformation path to be constructed with the convergence criterion satisfied for all load steps.

Table 1 Number of iterations and time of analysis for tangent stiffness approach.

		No. of Iterations for Convergence						
Integration Scheme	No. of Longitudinal Integration points	Step 2	Step 4	Step 6	Step 8	Step 10	Step 12	Analysis Time (Sec)
Gauss-Lobatto	4	3	9	4	7	3	4	0.015
Gauss-Lobatto	6	3	8	4	3	4	4	0.015
Gauss-Lobatto	8	3	9	8	4	8	5	0.015
Composite-Simpson	5	3	10	4	9	3	4	0.015
Composite-Simpson	11	3	8	8	4	8	5	0.031
Composite-Simpson	17	3	9	9	9	4	4	0.031

Table 2 Number of iterations and time of analysis for secant stiffness approach.

Integration Scheme	No. of Longitudinal Integration points	No. of Iterations for Convergence						Analysis Time (Sec)
		Step 2	Step 4	Step 6	Step 8	Step 10	Step 12	
Gauss-Lobatto	4	5	11	5	6	29	24	0.015
Gauss-Lobatto	6	5	9	5	5	34	30	0.015
Gauss-Lobatto	8	5	10	7	5	43	41	0.031
Composite-Simpson	5	5	10	4	8	29	24	0.015
Composite-Simpson	11	5	9	7	5	45	34	0.047
Composite-Simpson	17	5	9	9	8	41	38	0.062

The speed of solution as highlighted in Table 1 and 2 demonstrate the efficiency of the approach while maintaining accuracy.

5 Conclusions and recommendations

The general form of the flexibility method is derived by using the clamped cantilever configuration. The traditional concept of the fibre element at section level is replaced by a numerical integration to improve the formulation efficiency. The flexibility formulation in the framework of the tangent and secant stiffness is outlined and efficiency of the corresponding solution schemes has been demonstrated. Further work is currently being undertaken to include dynamic and impact loading.

References

[1] Banon, H., Biggs, J. M. & Irvine, H. M. (1981) Seismic damage in reinforced concrete frames. Vol. 107, No. 9, 1713-1729.

[2] Lai, S.-S., Will, G. T. & Otani, S. (1984) Model for inelastic biaxial bending of concrete members. Journal of Structural Engineering, Vol. 110, No. 11, 2563-2584.

[3] Tanaka, H. & Park, R., (1990). "Effect of lateral confining reinforcement on the ductile behaviour of reinforced concrete column". Report No. 90-2, University of Canterbury, Chrischurch, New Zealand.

[4] Marante, M. E. & Florez-Lopez, J. (2003) Three-dimensional analysis of reinforced concrete frames based on lumped damage mechanics. International Journal of Solids and Structures, Vol. 40, No. 19, 5109-5123.

[5] Hellesland, J. & Scordelis, A. C. (1981) Analysis of R.C. bridge columns under imposed deformations. Delft, Neth, IABSE, Zurich, Switz.

[6] Mari, A. & Scordelis, A. C., (1984). "Nonlinear geometric material and time dependent analysis of three dimensional reinforced and prestressed concrete frames". Report No. SESM 82-12, Department of Civil Engineering, University of California, Berkeley.

[7] Mahasuverachai, M., (1982). "Inelastic analysis of piping and tubular structures". Report No. EERC 82/27, Earthquake Engineering Research Centre, University of California, Berkeley,

[8] Marini, A. & Spacone, E. (2006) Analysis of reinforced concrete elements including shear effects. ACI Structural Journal, Vol. 103, No. 5, 645-655.

[9] Monti, G. & Spacone, E. (2000) Reinforced concrete fibre beam element with bond-slip. Journal of Structural Engineering, Vol. 126, No. 6, 654-661.

[10] Petrangeli, M., Pinto, P. E. & Ciampi, V. (1999) Fibre element for cyclic bending and shear of RC structures. I: theory. Journal of Engineering Mechanics, Vol. 125, No. 9, 994-1001.

[11] Taucer, F. F., Spacon, E. A. & Filippou, F. C., (1991). "A Fibre beam-column element for seismic response analysis of reinforced concrete structures". Report No. EERC 91/17, Earthquake Engineering Research Centre, University of California, Berkeley.

[12] Neuenhofer, A. & Filippou, F. C. (1997) Evaluation of nonlinear frame finite-element models. Journal of Structural Engineering, Vol. 123, No. 7, 958-966.

[13] Vali Pour, H. R. & Foster, S. J., (2007). "A Novel flexibility based beam-column element for nonlinear analysis of reinforced concrete frames". Report No. Uniciv Report, University of New South Wales, Sydney.

[14] Burns, N. H. & Siess, C. P., (1962). "Load-deformation characteristics of beam-column connections in reinforced concrete". Report No. SRS 234, University of Illinois, Urbana.